Journal of Glaciology

Article

Cite this article: Johnson A, Hock R, Fahnestock M (2021). Spatial variability and regional trends of Antarctic ice shelf surface melt duration over 1979–2020 derived from passive microwave data. *Journal of Glaciology* 1–14. https://doi.org/10.1017/jog.2021.112

Received: 13 January 2021
Revised: 30 September 2021
Accepted: 1 October 2021

Author for correspondence:
Andrew Johnson,
E-mail: acjohnson16@alaska.edu

cambridge.org/jog

Spatial variability and regional trends of Antarctic ice shelf surface melt duration over 1979–2020 derived from passive microwave data

Andrew Johnson[1], Regine Hock[1,2] and Mark Fahnestock[1]

[1]Geophysical Institute, University of Alaska Fairbanks, USA and [2]Department of Geosciences, University of Oslo, Norway

Abstract

Passive microwave satellite observations are used to identify the presence of surface meltwater across Antarctica at daily intervals from July 1979 to June 2020, with a focus on ice shelves. Antarctic Peninsula ice shelves have the highest number of annual days of melt, with a maximum of 89 days. Over the entire time period, there are few significant linear trends in days of melt per year. High melt years can be split into two distinct categories, those with high melt days in Dronning Maud Land and Wilkes Land, and those with high melt days in the Antarctic Peninsula and the Bellingshausen Sea sector of West Antarctica. The first pattern coincides with significant negative correlations between melt days and spring and summer Southern Annular Mode. Both patterns also form the primary modes of spatial and annual variability in the dataset observed by Principal Component Analysis. Areas experiencing extended melt for the first time in years tend to show large decreases in subsequent winter microwave emissions due to structural changes in the firn. We use this to identify the impact of novel melt events, particularly over the austral summers of 1991/92 and 2015/16 on the Ross Ice Shelf.

1. Introduction

Mass loss of the Antarctic ice sheet has the potential to surpass Greenland in contribution to sea-level rise by 2100 (Pörtner and others, 2019). The majority of potential Antarctic mass loss this century arises from ocean-driven and ice dynamic mechanisms (Golledge and others, 2019), yet surface melt is an increasing component of the mass budget as the atmosphere warms (DeConto and Pollard, 2016). While surface melt is largely restricted to the periphery of the ice sheet, with a mean annual extent over 2000–2009 of a mere 11% of the total surface area (melt over 1.47 million km^2, from Trusel and others (2012)), this area is comparable to the entire surface area of the Greenland Ice Sheet (1.7 million km^2). By the year 2100 some regions of Antarctica, especially the Antarctic Peninsula, could have surface melt rates similar to those found across the ablation area of Greenland during 2000–2009 (Bell and others, 2018) and surface melt across the entire continent in 2100 has the potential to equal that of Greenland during 2001–2006 (Trusel and others, 2015). Increasing melt is expected to result in mass loss due to increased runoff (Kittel and others, 2021), and surface melt is also related to dynamic ice loss mechanisms. Thinning ice shelves can collapse entirely due to melt pond driven hydrofracture (Scambos and others, 2009; Banwell and others, 2013) and the thinning and loss of ice shelves can reduce the backstress they provide on grounded ice which leads to glacier acceleration and thinning (e.g. Dupont and Alley, 2005). Surface meltwater reaching the bed has led to increased sliding resulting in acceleration of Antarctic Peninsula outlet glaciers (Tuckett and others, 2019).

Surface melt provides one key point of interaction between the Antarctic ice sheet and Antarctic climate. Over the past 50 years, atmospheric warming has not been uniform across Antarctica (Smith and Polvani, 2017). The Antarctic Peninsula has warmed very rapidly, with near-surface air temperatures at weather stations rising by up to 2.8°C from 1951 to 2000, and then slightly trending downward between 1999 and 2014 (Turner and others, 2016). Near-surface temperature reanalysis has revealed increasing West Antarctica temperatures from 1960 to 2010, while East Antarctica had few statistically significant temperature trends during that period (Nicolas and Bromwich, 2014). The drivers of climate variability can vary from one region to another. One important driver of coastal climate in East Antarctica is the poleward constriction of the Southern Westerly Winds, as measured by the Southern Annular Mode (SAM) (Marshall, 2007). The southward migration of the Southern Westerly Winds, which occurs during the positive SAM phase, has a cooling effect on East Antarctica and the Ross Sea sector of West Antarctica (Mayewski and others, 2009) and a warming effect on the Antarctic Peninsula. SAM has been trending positive since 1950, and is expected to continue to do so in a warming atmosphere (Bracegirdle and others, 2019). The El Niño Southern Oscillation (ENSO), which is defined by longitudinal pressure and temperature gradients across the Pacific, is known to bring warming and increased accumulation to the Antarctic Peninsula and parts of West Antarctica when in positive phase (El Niño), and

the negative phase (La Niña) is associated with decreased accumulation to West Antarctica (Paolo and others, 2018). The Antarctic climate patterns which are known to be related to times of strong ENSO have also been shown to be more intense when SAM was weak or in opposite phase with ENSO (Fogt and others, 2011).

Microwave-band satellite observations have provided data sources with application to the study of Antarctic surface melt. Passive microwave observations from radiometers have been used to quantify melt extent and duration across the entire Antarctic ice sheet and evaluate trends and climate teleconnections (e.g. Zwally and Fiegles, 1994; Torinesi and others, 2003; Picard and others, 2007; Tedesco and Monaghan, 2009), or investigate melt in individual regions of Antarctica (e.g. Fahnestock and others, 2002, and Banwell and others, 2021). From 2001 onwards the rapid-repeat scatterometers QuikSCAT and the Advanced SCATterometer (ASCAT) have been used to quantify melt extent and duration in Antarctica across the entire continent (Trusel and others, 2012; Bothale and others, 2015), or for specific regions (Barrand and others, 2013; Kuipers Munneke and others, 2018), or to quantify melt (Trusel and others, 2013). Similar near-daily melt detection has been shown to be possible for periods after 2014 with time series of high resolution, rapid-repeat Sentinel-1 SAR imagery (Johnson and others, 2020). However, many of the most pronounced melt events occurred during the 1990s, and thus were not covered by these recent active microwave records.

This work uses passive microwave satellite data to derive a 40-year time series of surface melt extent and duration across the Antarctic ice sheet over the period 1979–2020. We focus our analysis on melt on ice shelves because ice shelves provide the most ideal targets for passive microwave detection of melt with their low surface elevation and large extents, and also because ice shelves are especially susceptible to thinning, retreat and collapse in a warming climate (Gilbert and Kittel, 2021). This study adds an additional decade to previously published passive microwave melt records which allows us to reexamine previously reported trends and teleconnections. In particular, we analyze the characteristics of high melt years and compare these to the primary modes of variability in the spatial extent and duration of melt across all ice shelves. We demonstrate the relationship of the primary mode of variability to SAM. In addition, this work presents a new application of passive microwave time series to detect changes in firn stratigraphy due to abnormally high melt.

2. Methods

Snow and firn containing liquid water has a much greater emissivity than dry snow and firn, and therefore passive microwave observations are suitable for identifying the presence of meltwater at or close to a firn/snow surface (Mote and others, 1993). Passive microwave sensors measure upwelling thermal radiation. These observations are reported in brightness temperature (K), which is the temperature of a perfect black body required to produce the measured intensity of emissions.

Passive microwave melt detection methods make a binary assessment about the presence or absence of liquid water and days in which liquid water is detected are referred to as melt days. For each pixel of gridded daily (or every 2 day) passive microwave data in Antarctica, we compute the number of days per year in which melt can be detected (for simplicity henceforth referred to as annual melt days). A melt year here refers to July 1 through June 30 of the following calendar year in order to capture the austral summer. Melt days are quantified for every non-ocean pixel in Antarctica over the melt years 1979/1980 to 2019/20.

Most of the analysis here is focused on melt days on ice shelves. We specifically target pixels defined as having their entire 25×25 km^2 areal extent being categorized as ice shelf according to a SCAR coastline basemap (Fig. 1). Thus mixed pixels including surrounding non-ice shelf terrain are excluded to avoid pixels with high topographic variation at the sub-pixel scale and thus possible non-uniform melt within a single pixel (Johnson and others, 2020). Pixels which transitioned from ice shelf to ocean at some point during the time period due to ice shelf retreat or collapse were excluded, and we used year 2020 ice shelf outlines to determine ice shelf locations. One additional metric microwave studies in Antarctica have utilized to describe melt is a melt index defined by the product of area and number of melt days (e.g. Torinesi and others, 2003; Picard and others, 2007; Tedesco and others, 2007). In contrast, we report the number of annual melt days to allow for direct comparison of melt duration between ice shelves regardless of their size.

2.1. Data

We use passive microwave data collected by satellite-based passive microwave instruments from 1979 onwards. With wide swath widths of 783–1700 km, these microwave sensors in sun-synchronous orbit allow for daily (from 1987 on) and near-daily (1978–1987) observations. This study uses 18 and 19 GHz measurements in the horizontal polarization, as there is a high contrast between wet and dry firn in this frequency and polarization (Mote and others, 1993). These measurements are coarse in space, at a resolution approaching, but coarser than, the 25×25 km^2 pixel size which the data is posted at. An example of this processing method, and how it can sometimes lead to cross-contamination for nearby surfaces, is given in Gloersen (1992).

All passive microwave data were downloaded from the National Snow and Ice Datacenter (NSIDC). The Scanning Multi-channel Microwave Radiometer (SMMR) instrument on the Nimbus-7 satellite provided the data for 1979–1987 at 18.0 GHz (Gloersen and Francis, 2003). Since the SMMR observations imaged Antarctic ice shelves approximately only once every 2 days, a linear interpolation was used to fill in all missing days, regardless of gap length. The most important gaps in the record were during the 1986/87 austral summer, which had three separate gaps of 4 days in length during December and January. The Special Sensor Microwave Imager (SSM/I) and Special Sensor Microwave Imager/Sounder (SSMIS) instruments on board the Defense Meteorological Satellite Program satellites provided daily 19.35 GHz measurements from 1987 to 2020 (Meier and others, 2019). Due to a data gap of 40 days in December 1987 and January 1988 in the SSM/I record, the 1987/88 melt season was not considered in this study.

2.2. Melt detection

The emergence of meltwater in firn causes a drastic increase in the measured brightness temperature at 19 GHz, and this change is exploited to detect melt. The melt detection method used in this study follows Johnson and others (2020), which evaluated four different passive microwave melt detection algorithms across the Antarctic Peninsula by validating them against Sentinel-1 Synthetic Aperture Radar (SAR) melt observations. Sentinel-1 SAR has a resolution several orders of magnitude finer than the 25 km resolution of passive microwave observations. While the quantity of meltwater can vary greatly across ice shelves (e.g. Banwell and others, 2021), binary determinations of the presence of meltwater on ice shelves were found to be relatively uniform across the flat 25 km pixels. Overall, 98.9% of aggregated 1 km pixels in the SAR images shared the same melt or no melt determinations across individual 25 km passive microwave pixels on

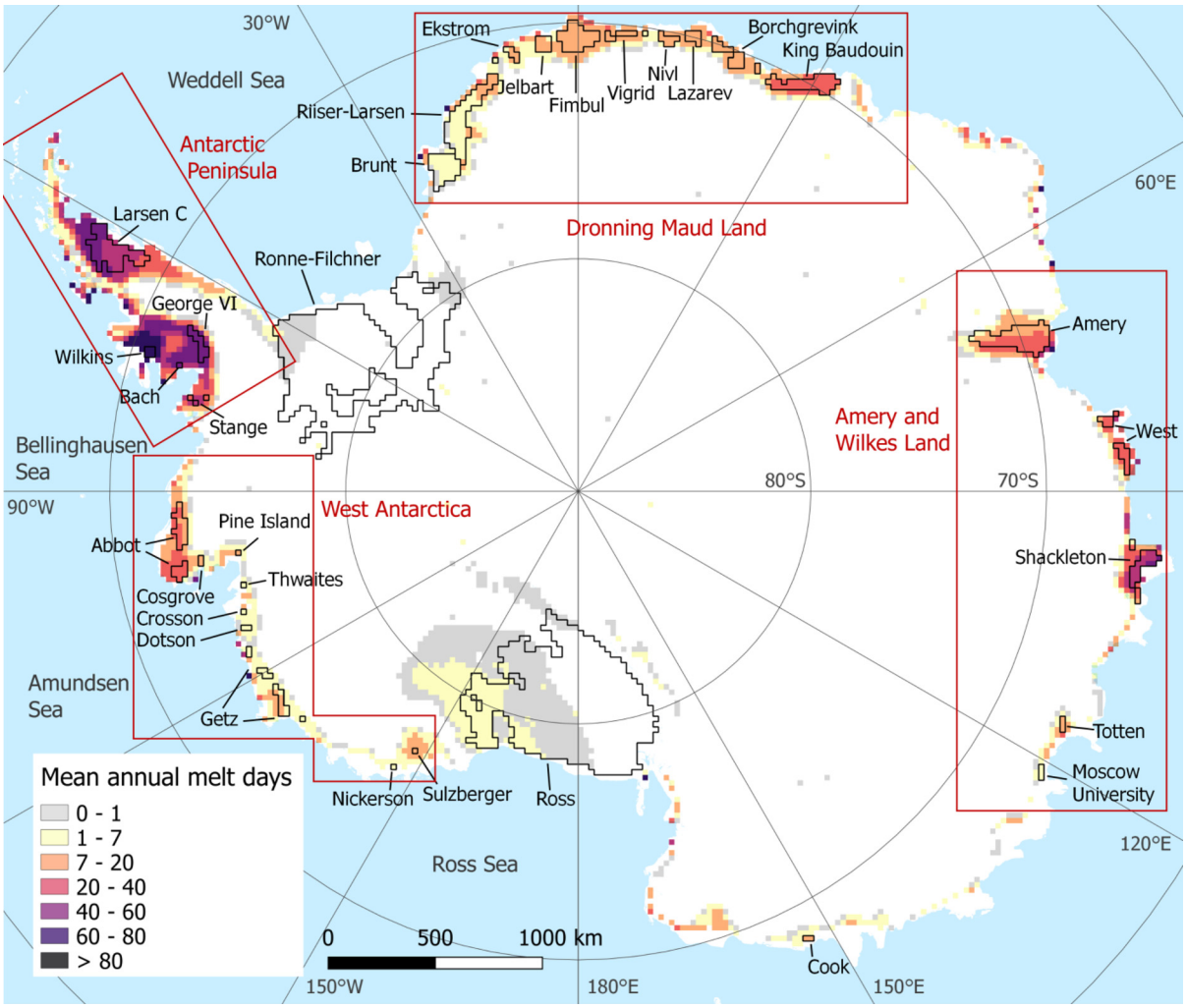

Fig. 1. Mean annual melt days for each passive microwave pixel across Antarctica, 1979–2020, using the K-means melt identification algorithm. Black outlines show the extent of each ice shelf used in further analyses (based on 25 × 25 km^2 pixels that are entirely classified as ice shelf).

ice shelves (Johnson and others, 2020). This result was much lower on the pixels surrounding ice shelves. The presence of meltwater was found to be much less uniform directly adjacent to ice shelves where there is often high topographic variation.

Of the four passive microwave methods compared by Johnson and others (2020), two of them used brightness temperature thresholds based on deviations from the previous winter's temperatures, including a 30 K increase threshold (Mote and others, 1993; Zwally and Fiegles, 1994) and a 3 standard deviation threshold (Torinesi and others, 2003). A third method used a cross-polarization gradient ratio (Abdalati and Steffen, 1997). A final method used a statistical analysis of brightness temperature time series using a K-means clustering algorithm. Here we use the latter method as it was found to be among the best correlated to SAR melt observations and was notably the least biased to overcount or undercount melt. During summer months, the SAR results agreed with this passive microwave method 88% of the time.

Comparison to 2 m air temperatures from Automated Weather Stations (AWS) was not carried out because there were few stations with continuous records on ice shelf surfaces which both experience notable melt and also experience the presence of meltwater uniformly at the 25 km resolution, aside from one station on the Larsen C Ice Shelf. In addition, liquid water can exist due to solar radiation in the surface when air temperatures are at or below 0°C (Tedesco, 2009) thereby complicating the validation technique.

This statistical method to detect melt used here applies a one-dimensional K-means clustering algorithm to the annual brightness temperature time series to identify two clusters. If that annual set of passive microwave observations fits well into two clusters on the brightness temperature axis, or the two cluster centers are far enough apart (set here at 40 K) then the upper cluster is identified as melt. A good two-cluster fit is defined as the root-mean-square distance of brightness temperatures to the nearest cluster center in the two cluster case being 42% that of the one cluster case. Otherwise, or if the two cluster centers are too close together (within 20 K), then a threshold brightness temperature of 40 K above the lower cluster is used to detect melt instead (see Johnson and others, 2020 for further details).

An additional filter was applied in order to remove any erroneous melt detections in either obviously dry firn or in pixels which bear time series partially resembling sea ice. On rare occasions dry firn pixels in parts of the interior of the ice sheet could fool the detection algorithm if their seasonal brightness temperature swings were large enough. Some coastal passive microwave pixels also had occasional years in the record in which their time series would partially resemble that of sea ice, as characterized by a sudden transition to extremely low brightness temperature values in mid-late summer indicating the presence of open ocean water, even in cases where the pixel itself covered only land or ice shelf. These could be the result of the formation of late melt season supraglacial lakes, which have been observed across Antarctica (Kingslake and others, 2017; Stokes and others, 2019; Arthur and others, 2020). However, not all instances of ice shelf pixels showing rapid transition to low summer brightness

temperatures align with observed instances of standing water on ice shelves, and in particular some of the strongest instances of this phenomena occur on the ocean-side of the Brunt Ice Shelf in the mid 1990s. To resolve this, we removed data from any individual pixel during a year if that pixel reported 90 more melt days than its mean annual melt days, or if the melt threshold brightness temperature was found to be <160 K. On the primary ice shelves used in this study, these criteria only applied to 0.22% of the individual pixel annual melt day totals.

This approach is designed to detect the large jumps in brightness temperatures due to the emergence of liquid water, which are much larger than the differences between satellites or instruments. As such we do not apply a calibration to the measured brightness temperatures of different satellites. To validate this approach however, we tested the passive microwave calibration detailed in Nicolas and others (2017), and we found that in the 6 years in which there was overlap between the satellites detailed in their calibration, only 0.06% of the annual melt day totals for ice shelf pixels were altered.

3. Results

3.1. Spatial variability of melt

The spatial distribution of annual melt days averaged over the period 1979–2020 is shown in Figure 1. As expected, there is a general pattern of decreasing melt days with distance from the ocean, often corresponding to increasing elevation. The region names given in the map will be referred to from here on. Results are shown for the entire Antarctic ice sheet but further analyses are focused on the ice shelves. While there are large areas outside the ice shelves with considerable melt days, many of these have significant topographic variation, and therefore are not likely to have a uniform presence of meltwater at the resolution of passive microwave. Annual melt days for individual ice shelf pixels vary between zero and 91 with an average of 24 days across all ice shelf pixels, excluding the Ross and the Ronne-Filchner ice shelves. On average, the Antarctic Peninsula ice shelves experience the most melt days, and only Antarctic Peninsula ice shelves and the Shackleton Ice Shelf have pixels which experience more than 60 mean annual melt days.

In Dronning Maud Land there is an overall west-to-east gradient of increasing annual melt days, consistent with Torinesi and others (2003), as well as regional climate models of surface melt (Van Wessem and others, 2018). Within the region, the westernmost Brunt and Riiser-Larsen ice shelves have the least melt days, with some pixels having less than one mean annual melt day, and the easternmost King Baudouin Ice Shelf has the most melt with up to 34 mean annual melt days. This gradient in melt days across the region likely indicates differing climate regimes across the region. For example, sea ice concentrations in western but not eastern Dronning Maud Land are strongly controlled by the Weddell Sea (Isaacs and others, 2021). In Amery and Wilkes Land the largest ice shelves, namely the Amery, West and Shackleton shelves, all have relatively high mean annual melt days with individual pixels exceeding 78 annual melt days. The ice shelves between the Moscow University and Cook ice shelves are smaller and have low melt day totals. Around the Cook Ice Shelf, there are many ice shelves which are too small for the coarse resolution of these passive microwave instruments to resolve.

On the western side of the continent, the Ross and Amundsen sea sectors of West Antarctica have few melt days. The most prominent ice shelf of the region, other than the Ross Ice Shelf, is the Getz Ice Shelf which has an area of ~10 000 km^2 observable by these passive microwave satellites and a mean of 5 annual melt days per pixel. Higher numbers of melt days are found in the Bellingshausen Sea sector. The Abbot is the largest ice shelf of the region with an investigated area of 15 000 km^2 and an average of 21 annual melt days. In the Antarctic Peninsula, all of the ice shelves have especially high annual melt days, with the George VI, Larsen C, and Wilkins Ice Shelf all averaging more than 50. In particular, the Wilkins Ice Shelf has the most melt days with individual pixels experiencing as many as 91 mean annual melt days. Pixels nearby to the Wilkins Ice Shelf reach up to 93 mean annual melt days. The annual melt day results we show on the Antarctic Peninsula are similar but slightly lower than those quantified over the same time period by Banwell and others (2021). Johnson and others (2020) demonstrate that on the Wilkins Ice shelf, the K-means statistical melt detection methods find a mean of 89 annual melt days over 1979/80-2018/19 whereas the method employed in Banwell and others (2021) finds 92 mean annual melt days.

3.2. Timing of melt

There are spatial patterns in the timing of melt across Antarctica, indicating earlier or later melt seasons in some regions. In order to quantify the timing of melt, we calculated the dates for the onset and midpoint of melt for each pixel. To quantify the onset of melt, we found the start date for the longest consecutive period of days of melt throughout the year with no gaps of 10 or more days. The midpoint of melt was the day of year on which half of all cumulative melt days had been reached, here referred to as melt day midpoint.

These results are shown in Figure 2. The earliest dates for the onset of melt on ice shelves occur in Amery and Wilkes Land and in the Antarctic Peninsula (Fig. 2a). The mean annual melt days of each pixel (Fig. 1) describe some of the variability in the timing of melt. Intuitively, pixels with more melt would usually be expected to have an earlier onset of melt. And indeed there is a significant negative correlation between pixel mean annual melt days and melt onset ($r = -0.94$, $p < 0.01$), equating more melt days with earlier onsets of the melt season. Throughout this paper, p-values are noted with either $p < 0.01$ or $p < 0.05$. To help track the spatial variability of timing of melt, Figure 2b shows the midpoint of melt for each pixel. There is also a low positive correlation between mean annual melt days and melt day midpoint day ($r = 0.29$, $p < 0.01$, Figs 1 and 2b), indicating that melt seasons often stretch further into the end of summer than the beginning for many regions with high melt, whereas low melt regions often experience melt seasons earlier in the summer, closer to the times of maximum possible solar radiation. These patterns are perhaps best exemplified in the Antarctic Peninsula, where there are long melt seasons and late midpoints of melt. There are two ice shelves however which are notable in that they defy this trend. The Shackleton and West ice shelves in Wilkes Land have high melt days and some of the earliest dates for the onset of melt, but they also have some of the earliest melt day midpoints. Therefore, these two ice shelves in Wilkes Land have an unusually early melt season compared to elsewhere across Antarctica.

The majority of melt days occurs during the summer, but several winter melt events have been documented, mostly on the Antarctic Peninsula. Figure 3 shows the mean annual melt days for each pixel during a winter period of April 15 to October 15 on the Antarctic Peninsula. There is large interannual variability in winter melt because a pixel might only experience winter melt events during a few years in the melt record. There is a correlation ($r = 0.60$, $p < 0.01$) between mean winter melt days and total mean melt days for each pixel as only pixels with relatively high amounts of melt ever see melt during the winter. However, further variability in winter melt days is likely related to specific

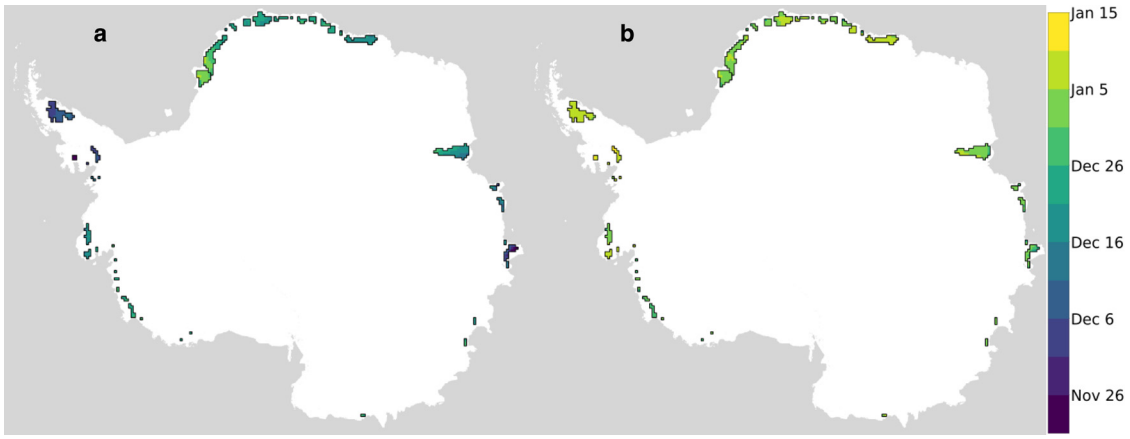

Fig. 2. (a) Mean day of onset of seasonal melt. (b) Day of year when half of the total number of annual melt days has been reached (here referred to as melt day midpoint). Results are averaged over 1979–2020.

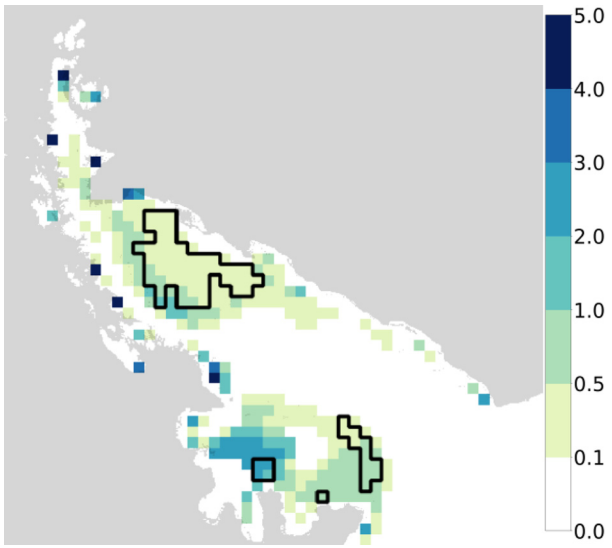

Fig. 3. Mean number of annual winter melt days for each pixel of the Antarctic Peninsula, over 1979–2019. The winter period here refers to 15 April–15 October.

local climatic processes. For example, Larsen C winter melt events have been shown to be driven by foehn winds (Kuipers Munneke and others, 2018; Datta and others, 2019) and the winter melt observed here occurs more frequently in the inland pixels where these foehn winds reach the shelf. These events range from a couple days up to 10 days on the Larsen C Ice Shelf (Kuipers Munneke and others, 2018). We find winter melt events on the Larsen C Ice Shelf with durations of up to 11 days. On the western side of the peninsula, winter melt days are most common to the west of the Wilkins ice shelf in regions closest to the Bellingshausen Sea. Temporally, there are almost no statistically significant linear trends in the number of days of winter melt over the four decade record ($p < 0.05$). This agrees with the lack of linear trends in winter melt days noted by Kuipers Munneke and others (2018) over 2000–2016 based on scatterometer observations.

3.3. Trends in annual melt days

Mean annual melt days over the 41-year study period are plotted for each investigated ice shelf in Figure 4, excluding the Ross and Ronne-Filchner ice shelves. Melt days averaged over all pixels on each ice shelf are shown. Interannual variability tends to be high, especially for many ice shelves with low annual melt day averages. For example, in most years, Thwaites has only a few days of melt per year, but there are 3 years in the record with more than 15 days of melt, reaching 30 days in 2012/13. The distribution of annual melt days detected by passive microwave instruments has been noted to appear gaussian for pixels with high melt days, and exponential for pixels with fewer melt days (Picard and others, 2007). High melt years are usually regionally coherent, and are further explored in Section 4.1.

None of the ice shelves in Figure 4 show a significant ($p < 0.05$) linear trend in annual melt days over the time period. Subsets of the time period have been demonstrated to show trends however, for example, Bothale and others, 2015 find significant negative trends over 2001–2014 using scatterometer data on some ice shelves, mostly clustered around the Antarctic Peninsula, with the Larsen C Ice Shelf seeing −3.3 days of melt per year. We do not find these trends to be significant in our data. Picard and others (2007) document negative trends in melt across the Antarctic Peninsula over 1995/96–2005/06. Over this time period, we find many individual pixels on the Larsen C Ice Shelf with significant negative melt day trends, with an average of −3.5 annual melt days per year ($p < 0.05$). As previously noted, the Antarctic Peninsula is observed having a negative annual temperature trend over 2000–2014 in the weather station temperature record (Turner and others, 2016).

Over the entire time period, if we consider the annual melt day time series of individual pixels instead of entire ice shelves, there are still few statistically significant linear trends over the time period. Across these ice shelves, only 4.1% of the individual passive microwave pixels have significant ($p < 0.05$) trends, and the linear trends that meet this threshold on ice shelves have a mean and standard deviation of -0.43 ± 0.12 annual melt days per year. These pixels are mostly spread across the Larsen C, Fimbul, Amery and Shackleton ice shelves. The significant trends range from −0.71 to −0.11 annual melt days per year.

The largest ice shelves, the Ronne-Filchner and the Ross, experienced very little melt. Their melt day time series is therefore shown separately in Figure 5. Melt is not spatially homogeneous across ice shelves this large, and even during the highest melt years, large swaths of the surface experienced no melt. Much of the surface of the Ronne-Filchner Ice Shelf experiences no melt in this record. On these ice shelves, melt primarily occurs on the northwestern section of the Ronne-Filchner Ice Shelf and the northeastern quadrant of the Ross Ice Shelf (Fig. 1). The vast majority of melt days on the Ross Ice Shelf are contained in just a few melt events, especially those during 1991/92 and 2015/16 (Fig. 5a). The median number of spatially averaged annual melt days across the Ross Ice Shelf is 0.08, yet the 1991/92 melt season averaged 7.6 melt days, and pixels in the northeast

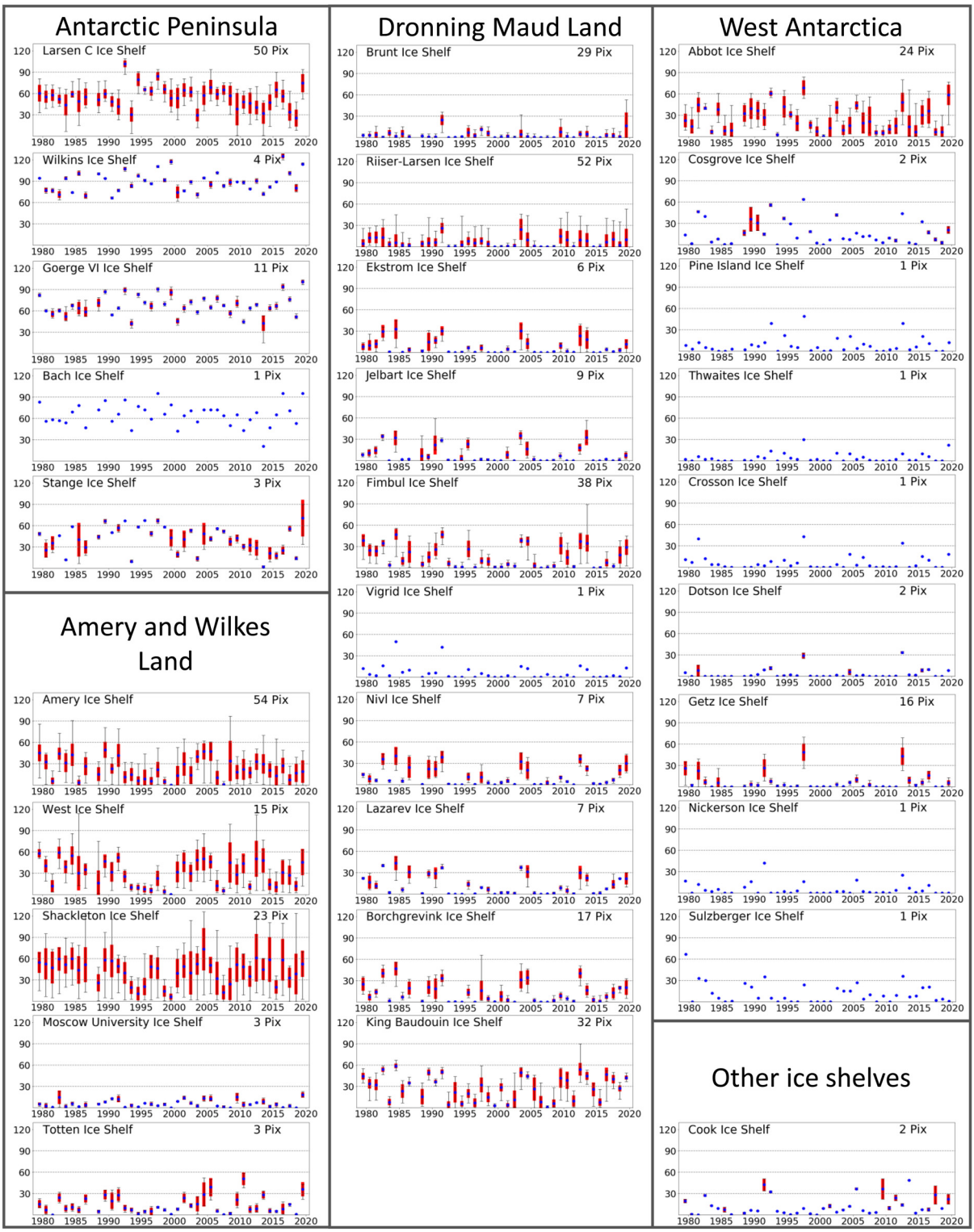

Fig. 4. Annual melt days for all 30 investigated Antarctic ice shelves from 1979/80 to 2019/20. Figure shows annual melt days averaged across all pixels of each ice shelf (as defined in Fig. 1), standard deviation (red bars) of pixels within that ice shelf, and range. Standard deviation and range markers are absent if the ice shelf only has one pixel or if all pixels have the same amount of melt. The Ross and Ronne-Filchner ice shelves are shown separately due to their much smaller number of melt days (Fig. 5).

showed melt for as many as 30 days. Further analysis of this melt event and its impacts are given in Section 4.3.

3.4. Spatial correlations

To investigate the spatial coherence of melt days across Antarctica, we correlate the mean annual melt day time series for each possible ice shelf pair. This comparison only correlates total annual melt days, with no regard to the timing of that melt throughout the year (further explored in Section 3.3). All of the significant correlations ($p < 0.05$) are shown in Figure 6, which account for 48% of all ice shelf pairs. The highest annual melt day correlations are found between ice shelves in the same region, which is to be expected. The greatest intra-region coherence was in Dronning Maud Land with correlation coefficients reaching up to 0.96. On the Antarctic Peninsula, the correlations

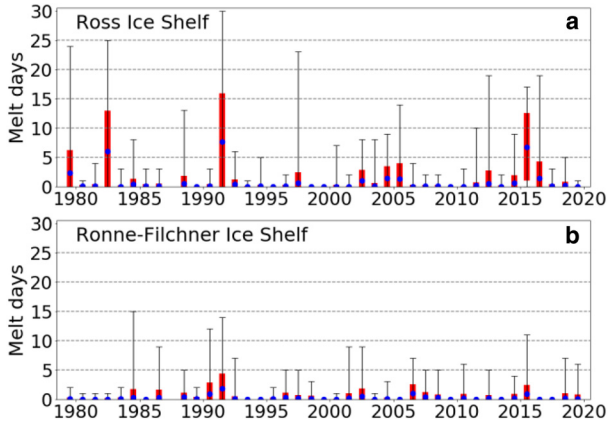

Fig. 5. Annual melt days averaged across all pixels on Ronne-Filchner and Ross ice shelves. Standard deviations given by red bars. The Ross Ice Shelf covers 647 pixels and the Ronne-Filchner covers 549 pixels.

between ice shelves on the western side of the mountainous spine is high (with r values as up to 0.93), but the correlations from the Larsen C on the eastern side to the other Antarctic Peninsula ice shelves are lower (r values of 0.40–0.65). Overall, correlation coefficients for ice shelves within each of the major regions in Figure 1 range from 0.31 to 0.96.

Perhaps more important to the study of climatic drivers are the correlations between regions. These correlations indicate that many ice shelves across the continent had similar very high or low melt day totals during the same years. Dronning Maud Land has relatively high correlations with Amery and Wilkes Land (with r values up to 0.71, averaging 2800 km apart) and West Antarctic ice shelves on the Ross Sea side of West Antarctica (with r values up to 0.55, 3000 km apart). The Ross Sea sector of West Antarctica also shows some correlations to Amery and Wilkes Land melt (r values up to 0.47), despite the fact that these regions are separated by an average distance of 4000 km. The Antarctic Peninsula has fewer melt day correlations with other regions. It has significant correlations with West Antarctica (r values up to 0.65) and also strikingly negative correlations with several Dronning Maud Land ice shelves across the Weddell Sea (with r values between −0.33 and −0.47) on the opposite side of the Weddell Gyre.

The spatial correlations of melt between ice shelves shown above demonstrate coherent temporal variations in melt days between many regions across the continent. In order to provide more detail so these results can be better compared to underlying climatic drivers, we compared the melt day time series of each individual pixel pair. We performed a Principal Component Analysis (PCA) to determine the primary modes of variability and visualize their spatial characteristics (Fig. 7) by using an eigen decomposition on the covariances between the annual melt day time series of each ice shelf pixel. The Ronne-Filchner and Ross ice shelves were excluded from this calculation because otherwise, due to their size, their faint modes of variability would dominate the PCA. These modes of variability imply a relationship of the climate drivers across the continent for that mode.

The first principal eigenvector (Fig. 7a) describes 41% of the variability in the annual melt day dataset, and has the strongest associations to Dronning Maud Land and Amery and Wilkes Land ice shelves, with a smaller negative connection to the Antarctic Peninsula. The second Principal Component (Fig. 7b) describes 20% of the variability and has strong associations to Antarctic Peninsula and Bellingshausen Sea sector ice shelves, but only a weak relationship to melt elsewhere on the continent. While the coefficients are negative in these regions instead of positive, it is the direction and not necessarily sign which shows the pattern of variability. The second mode implies that the strongest drivers of melt on the Antarctic Peninsula and West Antarctica have less impact on melt across the rest of Antarctica. These first two modes bear some visual resemblance to the East-West asymmetry of near-surface annual mean air temperature variability modes observed across Antarctica over 1958–2012 (Jun and others, 2020), although the temperature modes are strongly related to winter air temperature variability while surface melt here is primarily a summer phenomena. The third Principal Component is primarily dominated by the difference between melt in Amery and Wilkes Land to melt in Dronning Maud Land and accounts for 8% of the variability in the data. No other modes account for more than 5% of the variability.

4. Discussion

4.1. Analysis of high melt years

Many of the ice shelves around Antarctica have few spatially averaged melt days per year over 1979/80–2019/20, yet even in regions with very low melt there are notably abnormal years with remarkably high deviations from the mean. For example, the Getz Ice Shelf in the Amundsen Sea sector of West Antarctica (see Fig. 4 for the full melt record) experienced an average of 5 annual melt days. However, in each of the years of 1991/92, 1997/98 and 2012/13, there were more than 20 melt days. Similar ice shelves nearby, as well as many in Dronning Maud Land in 1991/92 and 2012/13, had very high melt days in those years as well. The climate characteristics of these remarkable years provide insight into the drivers of variability of melt days across Antarctica.

In this section, we identify years of high melt and categorize them. We classify a high melt year as a year in which three or more ice shelves have annual melt days of at least two standard deviations above their mean. There are eight melt years in the dataset which meet this criteria: 1982/83, 1984/85, 1991/92, 1992/93, 1997/98, 2003/04, 2012/13 and 2019/20. The years we identify here loosely fit into two categories: those which have a very high number of melt days in Dronning Maud Land (1982/83, 1984/85, 1991/92, 2003/04 and 2012/13), and those which have very high melt days on the Antarctic Peninsula and Bellingshausen Sea sector of West Antarctica (1992/93, 1997/98, 2019/20). The melt day anomalies relative to the 1979/80–2019/20 melt day average for each of these years are shown in Figure 8.

In the years with high numbers of melt days on Dronning Maud Land ice shelves, the ice shelves of Amery and Wilkes Land generally experienced similar anomalies but West Antarctica had variable melt days. The westernmost ice shelves of Dronning Maud Land, the Brunt and Riiser-Larsen, also did not have noticeably high or low melt during these years. The year 1991/92 stands out as it saw a remarkably high number of melt days on the Amundsen and Ross Ross Sea side of West Antarctica and also on the Ross Ice Shelf itself. One particularly notable pattern during these years is the contrast to the Antarctic Peninsula. During the five high melt years in Dronning Maud Land, the Antarctic Peninsula generally had negative melt day anomalies.

The pronounced spatial differences of melt days between Dronning Maud Land and the Antarctic Peninsula during these years are consistent with the negative correlations in annual melt days between these two regions (Figs 6a, b). Seven significant ($p < 0.05$) negative correlations were identified between ice shelf pairs in the Antarctic Peninsula and Dronning Maud Land, with r values ranging from −0.33 to −0.47. However, if these five

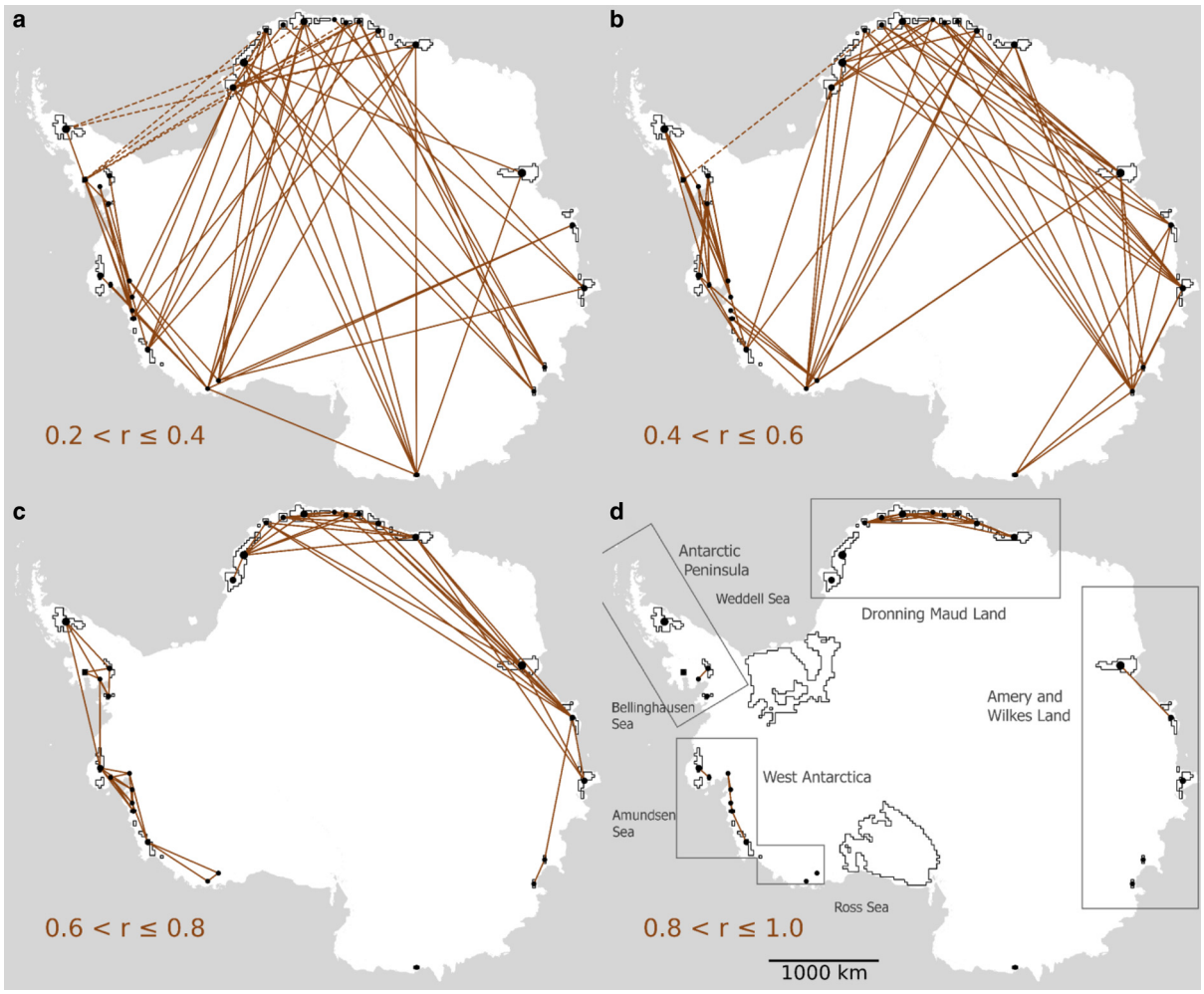

Fig. 6. Correlations (r) in annual melt days between ice shelves from 1979 to 2020 ($p < 0.05$). Ice shelves with statistically significant correlations are connected by lines, and results shown for four ranges of correlation coefficients. Positive correlations are given with solid lines, and negative correlations with dotted lines.

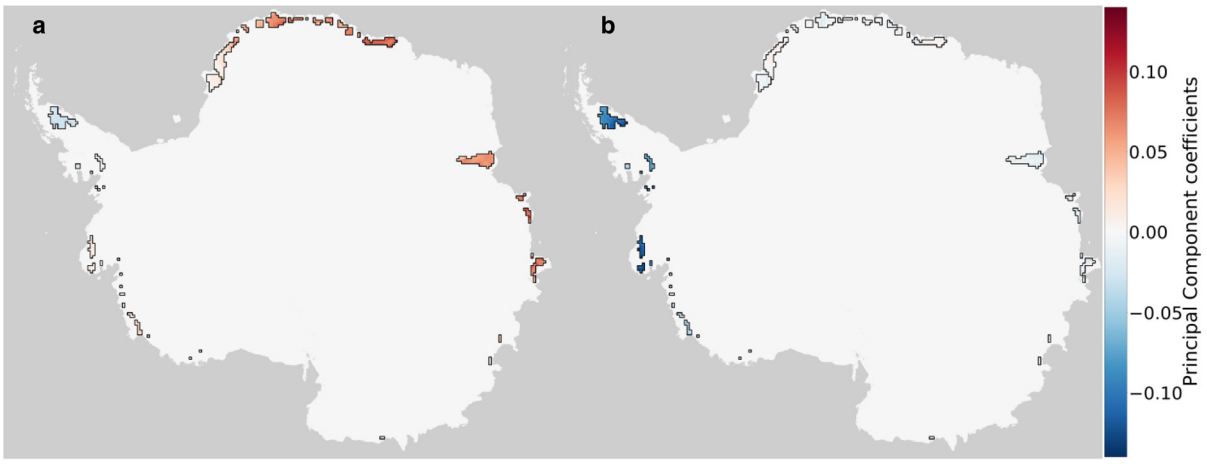

Fig. 7. First two Principal Components, with coefficients projected back onto their corresponding passive microwave pixels. (a) First Principal Component, which describes 41% of the variance. (b) Second Principal Component, which describes 20% of the variance.

particular years are removed from the record then all of the negative melt day correlations lose their statistical significance.

The years of 1992/93, 1997/98 and 2019/20 are marked by a notably high number of melt days on the Antarctic Peninsula and the Bellingshausen Sea sector of West Antarctica. Banwell and others (2021) note 1992/93 as having the highest cumulative melt on the Antarctic Peninsula. There are moderate to negative melt anomalies in Dronning Maud Land and Amery and Wilkes Land during these years. As shown in Figure 6, the annual melt days on the Antarctic Peninsula and Bellingshausen Sea side of the West Antarctica are not particularly correlated to melt days in other regions of Antarctica. Likewise in each of the years of 1992/93, 1997/98 and 2019/20, there are few distinct spatial patterns of melt days across the rest of the continent in each of those years.

The spatial patterns of melt days during these eight high melt years match closely with the direction of the first two Principal Components of melt day variability (Fig. 7). The spatial patterns

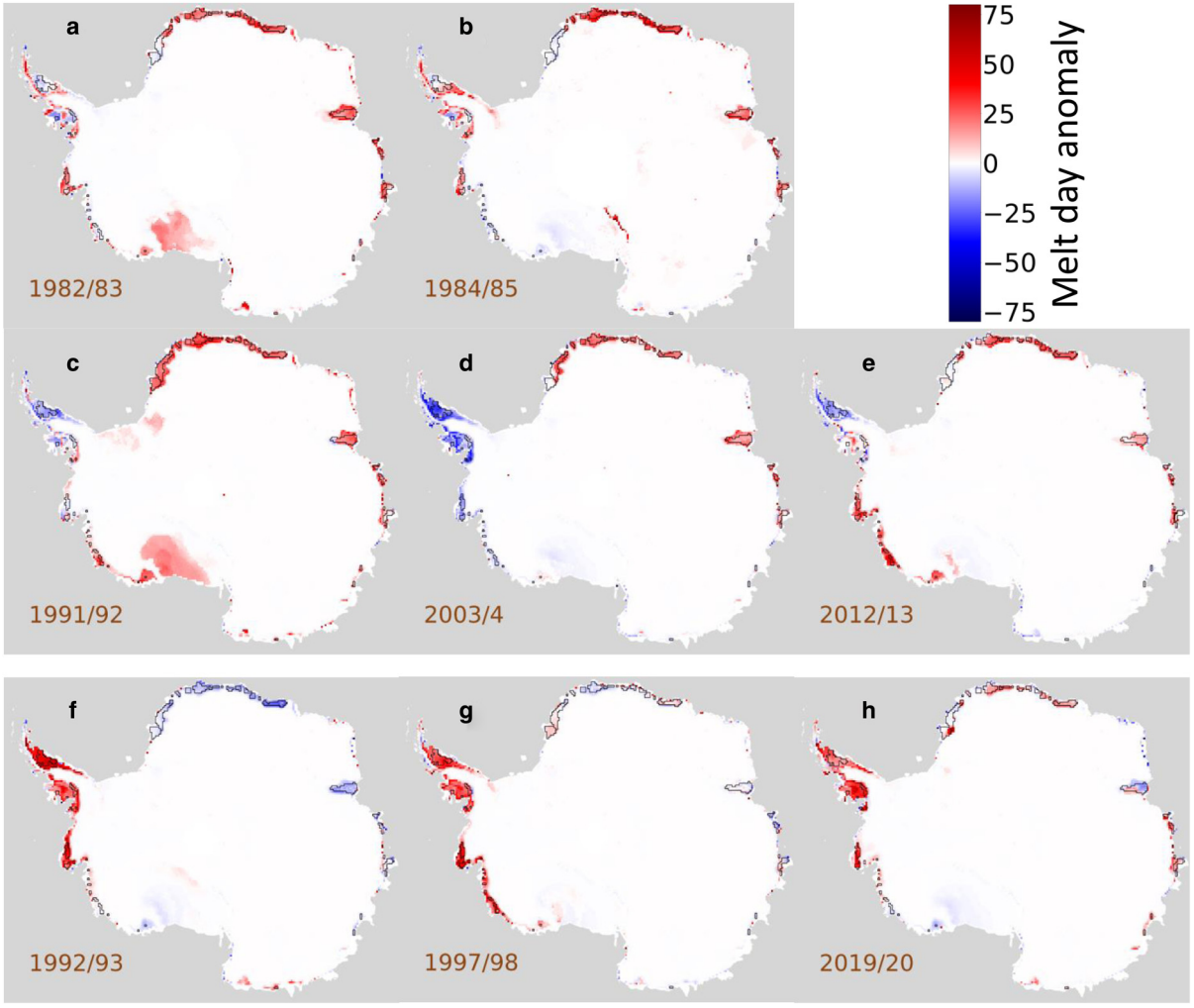

Fig. 8. Melt day anomaly relative to the 1979–2020 mean for each pixel for selected high melt years. Panels a–e show years with high melt day anomalies in Drowning Maud Land while panels f–h show years with high numbers of melt days on the Antarctic peninsula.

of melt during years with high melt days in Dronning Maud Land are similar to the first Principal Component of melt variability and the spatial patterns of melt in years with high melt on the Antarctic Peninsula show similarity to the second Principal Component, which is also dominated by the variability of the Antarctic Peninsula.

The years presented here mark the years with especially high melt along the ice shelves surrounding Antarctica. As such, a few years with notably high regional melt events or melt extents stretching further into the interior of the continent were not identified by this metric. In particular, we note 2005/06 which is documented as having especially high melt in the Amery, Wilkes Land and Ross regions of Antarctica (Tedesco, 2009), but not elsewhere. The 2015/16 melt season brought melt to a large extent of the Ross Ice Shelf and West Antarctica over a 1–2 week period in mid January, related to strong El Niño (Nicolas and others, 2017). During that year, there was some increased melt on the Abbot and Larsen C ice shelves, and decreased melt across Dronning Maud Land and Amery and Wilkes Land.

4.2. Climate correlations

To investigate the climatic context of the spatial variations in melt days across Antarctic ice shelves, we correlate the spatially averaged ice shelf annual melt day time series with ENSO as measured by the Multivariate ENSO Index (MEI) and SAM ($p < 0.05$). MEI and SAM values were obtained from the NOAA Physical Sciences Laboratory and NOAA Climate Prediction Center, respectively. Following previous literature (Torinesi and others, 2003; Tedesco, 2009), we compare melt days to the mean October through January climate index values as they were found to have some of the strongest correlations with melt detection results. All significant correlations are shown in Figure 9. Results show that many West Antarctica ice shelves, especially along the Amundsen Sea, have a moderate positive correlation (r values 0.32–0.49) with the mean October through January MEI. More substantial however in terms of r values and number of significant correlations are the correlations with SAM. In Dronning Maud Land, Amery and Wilkes Land, and West Antarctica, there are negative correlations (r values from −0.33 to −0.60) with the mean October through January SAM. The negative correlations with SAM are consistent with previous work (Torinesi and others, 2003; Tedesco, 2009), although their work found higher absolute correlations using melt area×day index values rather than melt days used here and without the benefit of the most recent decade of data. Picard and others (2007) also noted trends of decreasing melt days on the Antarctic Peninsula and increasing melt elsewhere coinciding with decreasing SAM.

Several lines of evidence suggest the importance of the role SAM plays in the variability of melt on Antarctic ice shelves. Many of the ice shelves in Figure 9 with the strongest negative

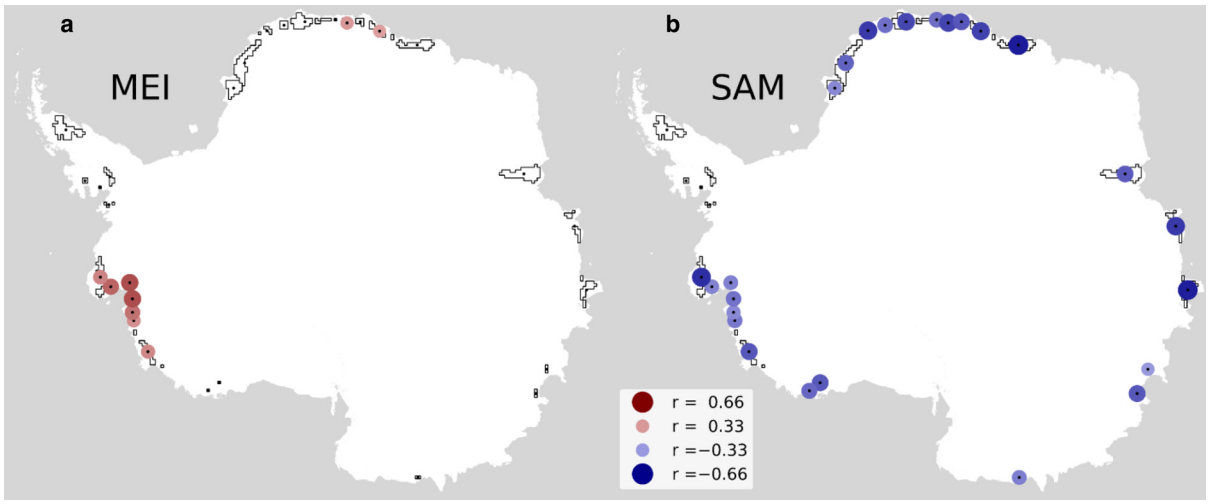

Fig. 9. Statistically significant correlation coefficients (*r*) between ice shelf annual melt days and mean October through January values of (a) the Multivariate ENSO Index and (b) the Southern Annular Mode. The radius and color of the circle scale with the absolute value of *r*. The maximum absolute *r* value is 0.60.

correlation of annual melt days to summertime SAM values are also the ice shelves with especially high melt during the large melt years of 1982/83, 1984/85, 1991/92, 2003/04 and 2012/13 (Fig. 8). These ice shelves, especially the ones in Dronning Maud Land and Amery and Wilkes Land, align with the first Principal Component of melt day variability in the PCA analysis (Fig. 7a). Furthermore, there is a direct relationship between SAM and the first PCA eigenvector. We tested the correlation of each individual passive microwave pixel on ice shelves to the mean October through January SAM values, and found that these correlations are also significantly correlated to the first Principal Component coefficients with an r value of -0.78 ($p < 0.01$). This demonstrates an inverse relationship in the southward migration of Southern Westerly Winds with melt days in Dronning Maud Land, such that there is more melt when these winds are further away from the continent. A similar but weaker connection is also found between the second Principal Component and MEI ($r = 0.12$, $p < 0.01$). Thus spring and summertime SAM values provide a major contribution to the primary mode of variability in the melt day record.

Firn core oxygen isotope analysis has shown that SAM was the dominant mode of climate variability in coastal Dronning Maud Land at the decadal scale over the past century (Naik and others, 2010). SAM provides an avenue to explain the physical mechanisms which could cause variability of Antarctic melt. The northward-migration of the Southern Westerly Winds associated with a negative summertime SAM phase is known to be related to increased warming in Dronning Maud Land and Amery and Wilkes Land as well as cooling in the Antarctic Peninsula (Marshall, 2007). We observe the melt dataset presented here to have a stronger relationship to SAM than to ENSO, although both are known to interact with Antarctic climate, and teleconnections to ENSO are strongest when SAM is weak or opposite (Fogt and others, 2011).

4.3. Detecting interannual changes to firn structure

For surfaces that normally have low numbers of melt days, we have frequently noticed changes to the microwave emission intensity of dry firn following summers with abnormally high melt. Figure 10 shows one such example on the Getz Ice Shelf. Over the entire 40-year time period, this pixel has a mean of 10 melt days per year, yet in the 2012/13 summer there was an unusually large melt event with a total of 45 melt days. Interestingly, after the melt had ended, the brightness temperature of the dry firn was significantly lower than it was before the melt season. This can be used to detect firn changes in some cases.

To quantify this effect, we define a value here called the Firn Seasonal Brightness Temperature Difference, Δ_{BT}, which is the mean September and October brightness temperature subtracted from the mean of the following March and April. This value is a measure of the change in brightness temperature caused by surface processes during the summer season. We observe that regions without melt, which is nearly the entire ice sheet except the periphery, on average have positive Δ_{BT} values indicating higher fall than spring brightness temperatures. We interpret this to be the result of the diffusion of seasonal heating into the snowpack. For example, the top several meters of a snowpack in dry firn in Antarctica have been observed to have higher temperatures in March–April than in September–October (e.g. Macelloni and others, 2007). Ice shelves and areas near the edge of the ice sheet which do experience melt however have negative Δ_{BT}. The decrease in Δ_{BT} in regions with melt is not necessarily linear with respect to the number of melt days. Regions which have more than 30 days of melt, such as the Antarctic Peninsula, do not have as large of a Δ_{BT} anomaly during very high melt years compared to areas which generally have much fewer melt days.

Several important anomalies of Δ_{BT} are given in Figure 11. The maps from 1991/92 and 1997/98 give examples of the Δ_{BT} anomaly during the two types of high melt years detailed in Section 4.1. The Ross Ice Shelf had large negative anomalies in 1991/92 and 2015/16, which are the years it experienced by far the most spatially cumulative melt days (Fig. 5a). On other parts of the continent, Dronning Maud Land had significant negative Δ_{BT} anomalies during 2003/04 and 2012/13 and West Antarctica had significant negative Δ_{BT} anomalies during 1997/98 and 2012/13. Each of these are years of especially high melt in those regions.

These decreases in firn brightness temperatures could be explained by increased grain growth and ice lens development due to melt. The effects of liquid water in a snowpack provide a physical basis for such a decrease in brightness temperature. Liquid water in firn promotes grain growth and can refreeze into ice lenses in the firn column (Benson, 1962). At 19 GHz, the upwelling radiation originates from the top several meters of a dry firn column, decreasing exponentially with depth (Chang and others, 1976). Ice lenses and larger snow grains increase microwave scattering in snow, thereby reducing the intensity of microwave emissions which can escape the firn after the melt concludes (Abdalati and Steffen, 1998). Microwave radar analysis of the 1991/92 Ross Ice Shelf event

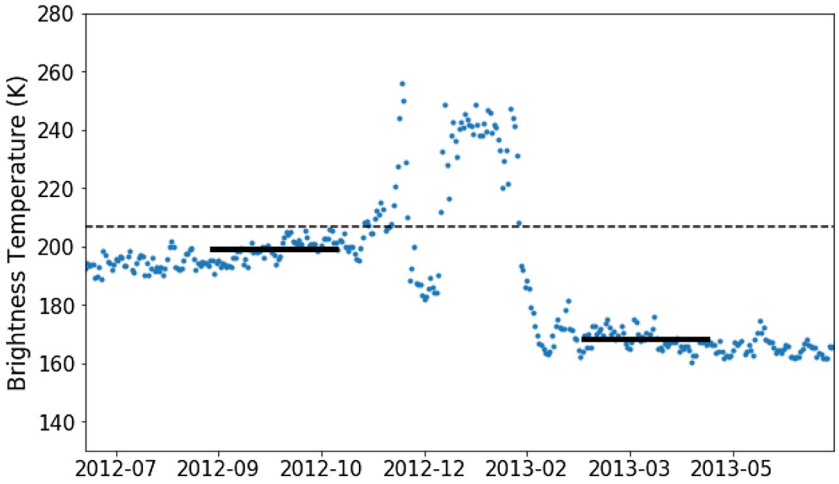

Fig. 10. Brightness temperature observations of single pixel on Getz Ice Shelf over the course of the austral summer 2012/13. Black lines indicate the mean value over the September–October and March–April periods used to detect changes in firn structure. Dashed line shows the melt detection threshold for this time series.

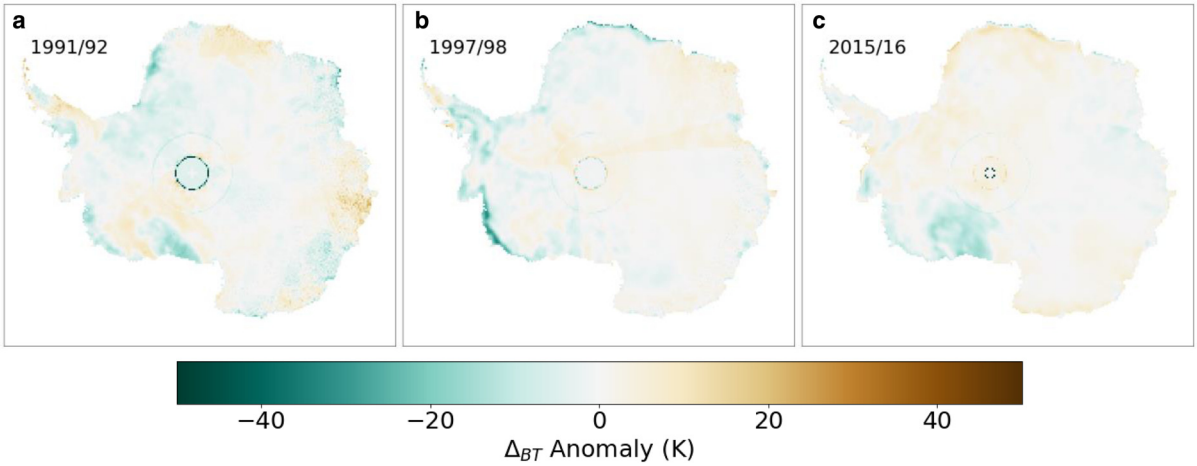

Fig. 11. Firn Seasonal Brightness Temperature Difference (Δ_{BT}) anomalies for select years.

has indicated the formation an ice layer (Fahnestock and Bamber, 2001), and firn cores on the Ross Ice Shelf taken in 1999–2001 mostly only had ice lenses associated with the 1991/92 melt season present in the core (Das and Alley, 2005), as well as a few lenses from the 1992/93 melt season. While we do not detect much melt overall melt on the Ross Ice Shelf during 1992/93 (Fig. 5a), there were some small melt events on the interior of the ice shelf (Fig. 8f) and there are coinciding negative Δ_{BT} anomalies in that region. The depressed dry firn brightness temperatures continued for more than a year in some cases. Burial rates at locations on the Ross Ice Shelf have been observed as being between 30 and 65 cm per year (Knuth and others, 2010), so ice lenses could take a couple years to be buried below the passive microwave observation depth.

To further aid this interpretation of abnormal brightness temperature decreases being related to melt-driven increases in grain growth and ice lens development in a firn surface, we have considered the scatterometer records of ASCAT over the 2015/16 melt event covering the Ross Ice Shelf. ASCAT Enhanced Resolution Images were obtained from the Scatterometer Climate Record Pathfinder at BYU. The January 2016 melt event has been well documented (Nicolas and others, 2017) and it appears clearly in the passive microwave melt record here (Fig. 12b). We compared two ASCAT images from directly before and after this melt event on the Ross Ice Shelf, and we observe a distinct increase in the ASCAT backscatter following this event, in the same spatial pattern as melt (Fig. 12a). Melt has been noted to create extremely strong microwave reflectors in a snowpack in the percolation zone of Greenland due to large snow grains and ice lenses (Rignot and others, 1993). The increase in backscatter on the Ross Ice Shelf over the 2015/16 austral summer is a clear indication of new scatters present in the firn column, and the spatial similarity to the melt event implicates the melt as the source of the scatterers. The melt features of ice lenses and increased grain sizes have already been noted to cause a decrease in the measured passive microwave brightness temperatures, and we observe the passive microwave Δ_{BT} decrease from this event on the Ross Ice Shelf (Fig. 12c) follows the same pattern as the melt and backscatter increases.

The annual Δ_{BT} anomalies could help to identify regions in which melt-driven changes occurred in these firn surfaces. Ice lens formation can increase runoff in a snowpack (Machguth and others, 2016), and the grain growth and ice lens development identified in this section can affect other microwave-band observations (Fig. 12a). These changes might pose problems for radar altimetry. For example, the radar altimetry-derived thinning rates on the Ross Ice Shelf observed by Paolo and others (2015) over 1994–1998 (their Fig. 2) have a spatial variability of up to 5 m a^{-1} across the Ross Ice Shelf with a pattern which closely aligns with the surface Δ_{BT} anomaly pattern from the 1991/92 melt season, despite thinning being attributed to basal melt. Ice lens development, detectable by changes in firn brightness temperature shown here, can contribute to changes in radar penetration depth over time, possibly leading to errors in analysis of active microwave radar time series.

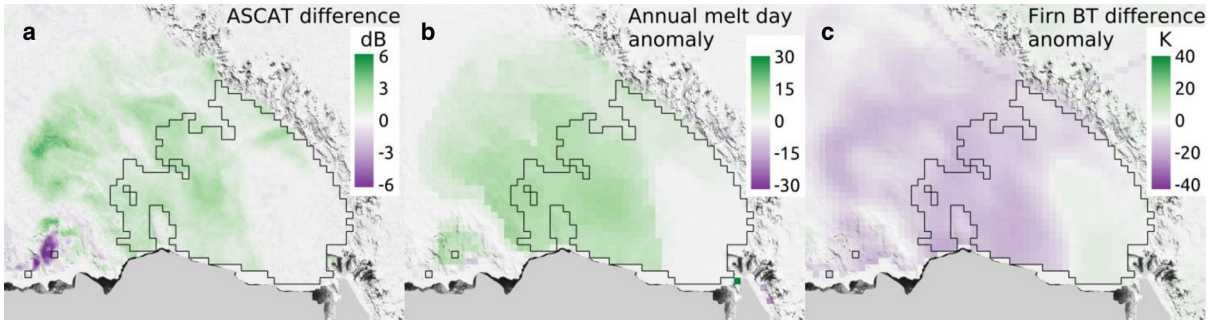

Fig. 12. Observations of the Ross ice shelf from the 2015/16 melt season. (a) ASCAT backscatter (σ^0) difference between 31 January 2016 and 1 January 2016. (b) Anomaly of annual melt day for 2015/16. (c) Anomaly of Firn Seasonal Brightness Temperature Difference (Δ_{BT}) anomaly for 2015/16. Background map is Modis Mosaic (Haran and others, 2014), with the passive microwave ice shelf mask outline shown.

5. Conclusions

Passive microwave datasets allow for quantification of melt days for the past four decades, providing a valuable dataset to augment other cryospheric observations. These results can be used to study climate across the continent or understand the recent history of a single ice shelf. Spatially the highest mean annual melt days occurred on the Wilkins Ice Shelf in the Antarctic Peninsula and the Shackleton Ice Shelf in Amery and Wilkes Land, with the Wilkins having the most at 89 mean annual melt days. In Dronning Maud Land, melt days show a positive eastward gradient, and West Antarctica also has similar spatial trend with generally increasing melt days eastward toward the Antarctic Peninsula.

Results show a striking lack of linear trends in the number of annual melt days over 1979–2020, despite the known positive trends in near-surface air temperatures across parts of the continent based on weather station records (Turner and others, 2020) and climate models (Smith and Polvani, 2017), or known negative trends in specific regions over specific time periods (Turner and others, 2016). Given the negative correlation of spring and summer SAM with melt days in Dronning Maud Land, Amery and Wilkes Land, and the Ross Sea sector of West Antarctica, the positive trend in SAM over this time period provides one mechanism which has been increasingly reducing annual melt days in these regions. Some of the divergences between the documented temperature trends and the results presented here may be explained by the fact that melt predominantly occurs during the summer. Regional and continent-wide trends in near-surface Antarctic temperatures have been shown to be weaker and less significant during the austral summer compared to other seasons, with spring having the highest trends (Nicolas and Bromwich, 2014).

Years with the highest melt can be classified into two groups, and these groups also match the primary modes of spatial and annual variability in the melt day dataset. Years with high numbers of melt days in Dronning Maud Land tend to have high melt days in Amery and Wilkes Land and in the Ross Sea sector of West Antarctica, as well as lower melt days on the Antarctic Peninsula. There are numerous correlations between the annual melt day time series for ice shelves in these regions, and they are similar to the pattern in the first Principal Component of melt day variability. This pattern has been further shown to be strongly (and inversely) related to October through January SAM, underscoring the importance of SAM, and therefore the constriction of the Southern Westerly Winds around Antarctica, during the austral spring and summer to ice shelf melt in these regions.

The years with the highest numbers of melt days in the Antarctic Peninsula and Bellingshausen Sea sector of West Antarctica lack spatial coherence of melt days elsewhere across the continent. There are few spatial correlations in the melt day time series between Antarctic Peninsula and Abbot ice shelves to ice shelves in other regions. The second Principal Component of melt day variability is the primary mode of variability for the Antarctic Peninsula, and it too shows little strength elsewhere. These results imply that the climate forces which cause high melt days on the Antarctic Peninsula are somewhat decoupled from the primary drivers of high melt days across the rest of Antarctica. We have also found mean October through January ENSO values to be positively correlated with melt days on many West Antarctic ice shelves, especially those in the Amundsen Sea sector.

The seasonal changes in firn brightness temperature, described here as Δ_{BT}, provide a useful tool for exploring changes to firn structure over time in regions which experience low amounts of melt. While this method does not quantify exact changes in grain size or ice lens thickness or frequency, it is the product of physical changes in the near-surface firn stratigraphy caused by melt. The grain growth and ice lens development captured by this metric is very likely observable in firn cores, as was noted on the Ross Ice Shelf. The record of Δ_{BT} anomalies can be used to aid in the study of firn development on many Antarctic ice shelves over this time period.

Acknowledgements. This study was support by National Science Foundation grant #1543432 and NASA grant #80NSSC17K0566. We thank the efforts of the two reviewers and scientific editor Carleen Tijm-Reijmer in improving the clarity and quality of this paper.

Data sources and availability. Coastline data were downloaded from SCAR Antarctica Digital Coastline Database (https://www.add.scar.org/), last accessed: 2020-01-09. SMMR data were downloaded from NSIDC (https://doi.org/10.5067/C8ZJDDHZAS59) (Gloersen and Francis, 2003). SSM/I and SSMIS data were downloaded from NSIDC (Meier and others, 2019). MEI values were downloaded from NOAA Physical Sciences Laboratory (https://psl.noaa.gov/enso/mei/), last accessed: 2020-11-2. SAM (AAO) data were provided by NOAA/National Weather Service Climate Prediction Center (https://www.cpc.ncep.noaa.gov/products/precip/CWlink/daily_ao_index/aao/aao.shtml), last accessed: 2020-10-26. ASCAT Enhanced Resolution Image Products were downloaded from Brigham Young University Scatterometer Climate Record Pathfinder (https://www.scp.byu.edu/data/Ascat/SIR/msfa/Ant.html), last accessed: 2021-4-17. MODIS Mosaic was downloaded from NSIDC (Haran and others, 2014). The melt day dataset produced for this study is available at https://doi.org/10.15784/601457.

References

Abdalati W and Steffen K (1997) Snowmelt on the Greenland Ice Sheet as derived from passive microwave satellite data. *Journal of Climate* **10**(2), 165–175.

Abdalati W and Steffen K (1998) Accumulation and hoar effects on microwave emission in the Greenland Ice-Sheet dry-snow zones. *Journal of Glaciology* **44**(148), 523–531.

Arthur JF, Stokes CR, Jamieson SS, Carr JR and Leeson AA (2020) Distribution and seasonal evolution of supraglacial lakes on Shackleton Ice Shelf, East Antarctica. *Cryosphere* **14**(11), 4103–4120.

Banwell AF and 7 others (2021) The 32-year record-high surface melt in 2019/2020 on the Northern George VI Ice Shelf, Antarctic Peninsula. *Cryosphere* **15**(2), 909–925.

Banwell AF, MacAyeal DR and Sergienko OV (2013) Breakup of the Larsen B Ice Shelf triggered by chain reaction drainage of supraglacial lakes. *Geophysical Research Letters* **40**(22), 5872–5876.

Barrand N and 6 others (2013) Trends in Antarctic Peninsula surface melting conditions from observations and regional climate modeling. *Journal of Geophysical Research. Earth Surface* **118**(1), 315–330.

Bell RE, Banwell AF, Trusel LD and Kingslake J (2018) Antarctic surface hydrology and impacts on ice-sheet mass balance. *Nature Climate Change* **8**(12), 1044–1052.

Benson C (1962) Stratigraphic studies in the snow and firn of Greenland Ice Sheet, CRREL (SIPRE) research report 70.

Bothale RV, Rao P, Dutt C, Dadhwal V and Maurya D (2015) Spatio-temporal dynamics of surface melting over Antarctica using OSCAT and QuikSCAT scatterometer data (2001–2014). *Current Science* **1**, 733–744.

Bracegirdle TJ and 9 others (2019) Back to the future: using long-term observational and paleo-proxy reconstructions to improve model projections of Antarctic climate. *Geosciences Journal* **9**(6), 255.

Chang T, Gloersen P, Schmugge T, Wilheit T and Zwally H (1976) Microwave emission from snow and glacier ice. *Journal of Glaciology* **16**(74), 23–39.

Das SB and Alley RB (2005) Characterization and formation of melt layers in polar snow: observations and experiments from West Antarctica. *Journal of Glaciology* **51**(173), 307–312.

Datta RT and 6 others (2019) The effect of foehn-induced surface melt on firn evolution over the Northeast Antarctic Peninsula. *Geophysical Research Letters* **46**(7), 3822–3831.

DeConto RM and Pollard D (2016) Contribution of Antarctica to past and future sea-level rise. *Nature* **531**(7596), 591–597.

Dupont T and Alley RB (2005) Assessment of the importance of ice-shelf buttressing to ice-sheet flow. *Geophysical Research Letters* **32**(4), L04503.

Fahnestock MA, Abdalati W and Shuman CA (2002) Long melt seasons on ice shelves of the Antarctic Peninsula: an analysis using satellite-based microwave emission measurements. *Annals of Glaciology* **34**, 127–133.

Fahnestock M and Bamber J (2001) Morphology and surface characteristics of the West Antarctic ice sheet. *The West Antarctic ice sheet: behavior and environment. Washington, DC, American Geophysical Union*, 13–27.

Fogt RL, Bromwich DH and Hines KM (2011) Understanding the sam influence on the South Pacific ENSO teleconnection. *Climate Dynamics* **36**(7-8), 1555–1576.

Gilbert E and Kittel C (2021) Surface melt and runoff on Antarctic ice shelves at 1.5°c, 2°c and 4°c of future warming. *Geophysical Research Letters* **48**(8), e2020GL091733.

Gloersen P (1992) *Arctic and Antarctic sea ice, 1978-1987: satellite passive-microwave observations and analysis*. 511, Scientific and Technical Information Program, National Aeronautics and Space Administration.

Gloersen P and Francis EA (2003) Nimbus-7 SMMR antenna temperatures. NASA National Snow and Ice Data Center Distributed Active Archive Center, Version 1, South 18H and 37V. Doi: https://doi.org/10.5067/C8ZJDDHZAS59. Last accessed: 2017-7-19.

Golledge NR and 6 others (2019) Global environmental consequences of twenty-first-century ice-sheet melt. *Nature* **566**(7742), 65–72.

Haran T, Bohlander J, Scambos T, Painter T and Fahnestock M (2014, updated 2019) Modis mosaic of antarctica 2008-2009 (moa2009) image map, version 1. NSIDC: National Snow and Ice Data Center Distributed Active Archive Center, Version 1 South 19H and 37V. Doi: https://doi.org/10.7265/N5KP8037. Last accessed: 2020-2-7.

Isaacs FE, Renwick JA, Mackintosh AN and Dadic R (2021) ENSO modulates summer and autumn sea ice variability around Dronning Maud Land, Antarctica. *Journal of Geophysical Research. Atmospheres* **126**(5), e2020JD033140.

Johnson A, Fahnestock M and Hock R (2020) Evaluation of passive microwave melt detection methods on Antarctic Peninsula ice shelves using time series of Sentinel-1 SAR. *Remote Sensing of Environment* **250**, 112044.

Jun SY and 5 others (2020) The internal origin of the west-east asymmetry of Antarctic climate change. *Science Advances* **6**(24), eaaz1490.

Kingslake J, Ely JC, Das I and Bell RE (2017) Widespread movement of meltwater onto and across Antarctic ice shelves. *Nature* **544**(7650), 349–352.

Kittel C and 9 others (2021) Diverging future surface mass balance between the Antarctic ice shelves and grounded ice sheet. *Cryosphere* **15**(3), 1215–1236.

Knuth SL, Tripoli GJ, Thom JE and Weidner GA (2010) The influence of blowing snow and precipitation on snow depth change across the Ross Ice Shelf and Ross Sea regions of Antarctica. *Journal of Applied Meteorology and Climatology* **49**(6), 1306–1321.

Kuipers Munneke P and 9 others (2018) Intense winter surface melt on an Antarctic ice shelf. *Geophysical Research Letters* **45**(15), 7615–7623.

Macelloni G, Brogioni M, Pampaloni P and Cagnati A (2007) Multifrequency microwave emission from the Dome-C area on the East Antarctic plateau: temporal and spatial variability. *IEEE Transactions on Geoscience and Remote Sensing* **45**(7), 2029–2039.

Machguth H and 9 others(2016) Greenland meltwater storage in firn limited by near-surface ice formation. *Nature Climate Change* **6**(4), 390–393.

Marshall GJ (2007) Half-century seasonal relationships between the southern annular mode and Antarctic temperatures. *International Journal of Climatology* **27**(3), 373–383.

Mayewski PA and 9 others (2009) State of the Antarctic and southern ocean climate system. *Reviews of Geophysics (Washington, D.C.* **47**(1), RG1003.

Meier WN, Wilcox H, Hardman MA and Stewart JS (2019) DMSP SSM/I-SSMIS daily polar gridded brightness temperatures. National Snow and Ice Data Center Distributed Active Archive Center, Version 5, South 19H and 37V. Doi: https://doi.org/10.5067/QU2UYQ6T0B3P. Last accessed:2020-12-24.

Mote TL, Anderson MR, Kuivinen KC and Rowe CM (1993) Passive microwave-derived spatial and temporal variations of summer melt on the Greenland Ice Sheet. *Annals of Glaciology* **17**, 233–238.

Naik SS, Thamban M, Laluraj C, Redkar B and Chaturvedi A (2010) A century of climate variability in central Dronning Maud Land, East Antarctica, and its relation to southern annular mode and El niño-southern oscillation. *Journal of Geophysical Research Atmospheres* **115**(D16), D16102.

Nicolas JP and Bromwich DH (2014) New reconstruction of Antarctic near-surface temperatures: multidecadal trends and reliability of global reanalyses. *Journal of Climate* **27**(21), 8070–8093.

Paolo FS, Fricker HA and Padman L (2015) Volume loss from Antarctic ice shelves is accelerating. *Science (New York, N.Y.)* **348**(6232), 327–331.

Picard G, Fily M and Gallée H (2007) Surface melting derived from microwave radiometers: a climatic indicator in Antarctica. *Annals of Glaciology* **46**, 29–34.

Pörtner H and 12 others (2019) *IPCC special report on the ocean and cryosphere in a changing climate*. IPCC.

Scambos T and 9 others (2009) Ice shelf disintegration by plate bending and hydro-fracture: satellite observations and model results of the 2008 Wilkins Ice Shelf break-ups. *Earth and Planetary Science Letters* **280**(1-4), 51–60.

Smith KL and Polvani LM (2017) Spatial patterns of recent Antarctic surface temperature trends and the importance of natural variability: lessons from multiple reconstructions and the CMIP5 models. *Climate Dynamics* **48**(7-8), 2653–2670.

Stokes CR, Sanderson JE, Miles BW, Jamieson SS and Leeson AA (2019) Widespread distribution of supraglacial lakes around the margin of the East Antarctic ice sheet. *Scientific Reports* **9**(1), 1–14.

Tedesco M (2009) Assessment and development of snowmelt retrieval algorithms over Antarctica from K-band spaceborne brightness temperature (1979–2008). *Remote Sensing of Environment* **113**(5), 979–997.

Tedesco M, Abdalati W and Zwally H (2007) Persistent surface snowmelt over Antarctica (1987–2006) from 19.35 GHz brightness temperatures. *Geophysical Research Letters* **34**(18), L18504.

Tedesco M and Monaghan AJ (2009) An updated Antarctic melt record through 2009 and its linkages to high-latitude and tropical climate variability. *Geophysical Research Letters* **36**(18), L18502.

Torinesi O, Fily M and Genthon C (2003) Variability and trends of the summer melt period of Antarctic ice margins since 1980 from microwave sensors. *Journal of Climate* **16**(7), 1047–1060.

Trusel LD and 6 others (2015) Divergent trajectories of Antarctic surface melt under two twenty-first-century climate scenarios. *Nature Geoscience* **8**(12), 927–932.

Trusel L, Frey KE and Das SB (2012) Antarctic surface melting dynamics: enhanced perspectives from radar scatterometer data. *Journal of Geophysical Research. Earth Surface* **117**(F2), F02023.

Trusel LD, Frey KE, Das SB, Munneke PK, Van Den Broeke MR (2013) Satellite-based estimates of Antarctic surface meltwater fluxes. *Geophysical Research Letters* **40**(23), 6148–6153.

Tuckett PA and 6 others (2019) Rapid accelerations of Antarctic Peninsula outlet glaciers driven by surface melt. *Nature Communications* **10**(1), 1–8.

Turner J and 9 others (2016) Absence of 21st century warming on Antarctic Peninsula consistent with natural variability. *Nature* **535**(7612), 411–415.

Turner J and 5 others (2020) Antarctic temperature variability and change from station data. *International Journal of Climatology* **40**(6), 2986–3007.

Van Wessem JM and 9 others (2018) Modelling the climate and surface mass balance of polar ice sheets using RACMO2–part 2: Antarctica (1979–2016). *Cryosphere* **12**(4), 1479–1498.

Zwally HJ and Fiegles S (1994) Extent and duration of Antarctic surface melting. *Journal of Glaciology* **40**(136), 463–475.